Computational and Experimental Studies on a Moving Ion Exchange Bed

Shinichiro Gondo[1]
Department of Chemical Engineering, Kyushu University, Fukuoka, Japan

Masato Itai
Mitsui Shipbuilding and Engineering Co., Ltd., Tokyo, Japan

Koichiro Kusunoki
Department of Chemical Engineering, Kyushu University, Fukuoka, Japan

Transient and steady-state conditions of a moving ion exchange bed were studied using an ion exchange system of 0.1*N* NaCl and Amberlite IR-120(H^+). The experimental results showed that at steady state the concentration of the outlet liquid is only a function of the ratio of the rate of flow of liquid to that of the resin particles. For the transient state the time required for obtaining steady state is 130 to 400 times as much as the residence time of the liquid in the column, increasing with a decrease in the ratio of flow rates. To simulate a moving ion exchange bed by digital computations, a numerical method was derived for solving the partial differential equations representing a material balance. Simulations by this method were able to predict fairly well the outlet liquid concentrations observed in the experiments.

Although ion exchange processes have usually been carried out using fixed beds, semicontinuous countercurrent moving beds have also been used in treatment of water and of nuclear reactor fuel. The equipment used for semicontinuous ion exchange operations has been constructed so that the fluid comes in contact with the ion exchange resin particles after each bed movement. The Higgins contactor is a typical example of such equipment. Details were reported by Hancher and Jury (1959). Several papers have been published on continuous ion exchange processes (Drake and Peebles, 1957; Hiester, 1951; Hiester and Phillips, 1953; Hiester *et al.*, 1954; Higgins, 1956). These authors studied correlations of mass transfer data at steady state or the operational performance of equipment for uranium recovery from ore leach solution.

This paper discusses the computational predictions of the transient and steady state of a moving ion exchange bed for an aqueous solution of sodium chloride and a strong cation exchange resin, Amberlite IR-120, prepared by the Rohm and Haas Co. The resin was in the hydrogen form. The liquid concentrations were such that the mass transfer rate was controlled by the resistance of the liquid phase. The authors first studied experimentally the effect of the flow rate of the liquid and the resin particles and the period of cyclic operations on the transient and steady state. They then derived a numerical solution for the partial differential equation of the material balances and compared the results of the calculations with experimental data.

Theory

Numerical Treatment of Partial Differential Equations of Material Balance. The ion exchange process has been considered to consist of four steps.

1. Transfer of the ion to be adsorbed to the surface of the ion exchange resin particles through the liquid film
2. Diffusion of the ion within the resin particle
3. Ion exchange reaction
4. Diffusion of the exchanged ion away from the site

The rate of the third step may be sufficiently faster than the others. Therefore, its contribution to the over-all transfer resistance may be negligible. Whether step 1 or steps 2 and 4 control the mass transfer rate depends on the operating conditions and the system used. In this investigation, the first step was regarded as the rate-determining step through all of the moving bed runs. Therefore, the material balance equations are derived here for the case where the film resistance is controlling.

Consider the exchange system where the sodium ion in the liquid replaces the hydrogen ion in the resin particles. The ion exchange reaction is expressed by

$$Na^+ + R - H \rightleftharpoons R - Na + H^+ \qquad (1)$$

When the equivalent fractions of the sodium ion in the liquid and in the resin are designated by x and y, respectively, the selectivity coefficient for this system, K, is given by Equation 2 in terms of x and y under equilibrium conditions.

$$K = \frac{y \cdot (1 - x)}{x \cdot (1 - y)} \qquad (2)$$

When the positive direction of the axis of the moving bed column is taken along that of the liquid flow through the column, the material balances around the infinitesimal bed height, Z, are represented as follows:

$$\epsilon C_\Sigma \frac{\partial x}{\partial t} + (1 - \epsilon)Q \frac{\partial y}{\partial t} + u_F C_\Sigma \frac{\partial x}{\partial Z} = 0 \qquad (3)$$

$$(1 - \epsilon)Q \frac{\partial y}{\partial t} = k_F a C_\Sigma (x - x_s) \qquad (4)$$

[1] To whom correspondence should be sent.

According to the assumption that the first step is rate-determining, there should be an equilibrium relation between x_s and y. From Equation 2 we obtain

$$x_s = \frac{y}{K(1 - y) + y} \tag{5}$$

In applying these equations to the moving bed operation, Equations 3, 4, and 5 must be solved simultaneously for the liquid flow period and then the concentration distributions at the end of the liquid flow period must be moved along the direction of bed moving to the bed height, Z_m, which is occupied by the fresh resin particles fed after every portion of liquid flow. In other words, the concentration distributions obtained in this way become the initial conditions for the next period. The phenomena of the moving bed operation can be represented theoretically by repeating these procedures.

As the equilibrium relation given by Equation 5 is nonlinear and the initial conditions for each period may be given only by numerical values, the simultaneous solution of Equations 3, 4, and 5 must be performed numerically. Hence, these equations must be rewritten in difference form. In the following, Δt and ΔZ mean the time and the axial increment, respectively, and i and j mean the number of increments of ΔZ and Δt, respectively. Figure 1 is a diagram of the process, using notations that appear in the following equations.

Replacing the second term of the left side of Equation 3 by the right side of Equation 4, we obtain the following difference equation.

$$\epsilon C_\Sigma \frac{x_{i,j+1} - x_{i,j}}{\Delta t} + k_F a C_\Sigma (x_{i,j+1} - x_{si,j+1}) + u_F C_\Sigma \frac{x_{i+1,j+1} - x_{i,j+1}}{\Delta Z} = 0 \tag{6}$$

From Equation 4, we obtain

$$(1 - \epsilon) Q \frac{y_{i,j+1} - y_{i,j}}{\Delta t} = k_F a C_\Sigma (x_{i,j} - x_{si,j}) \tag{7}$$

From Equation 5, we obtain

$$x_{si,j+1} = \frac{y_{i,j+1}}{K(1 - y_{i,j+1}) + y_{i,j+1}} \tag{8}$$

Equations 6 and 7 are solved for $x_{i+1,j+1}$ and $y_{i,j+1}$, respectively.

$$x_{i+1,j+1} = (1 - F_1 - F_2) x_{i,j+1} + F_1 x_{i,j} + F_2 x_{si,j+1} \tag{9}$$

$$y_{i,j+1} = F_3 (x_{i,j} - x_{si,j}) + y_{i,j} \tag{10}$$

where

$$\left.\begin{aligned} F_1 &= \frac{\epsilon \Delta Z}{u_F \Delta t} \\ F_2 &= \frac{k_F a \Delta Z}{u_F} \\ F_3 &= \frac{k_F a C_\Sigma \Delta t}{(1 - \epsilon) Q} \end{aligned}\right\} \tag{11}$$

The conditions for Equation 9 to give $x_{i+1,j+1}$ a positive value not greater than unity are that every coefficient appearing in the right side of Equation 9 is positive and not greater than unity, assuming that each x in the right side is positive and not greater than unity—that is,

$$\left.\begin{aligned} 0 < F_1 + F_2 < 1 \\ 0 < F_1, \quad F_2 < 1 \end{aligned}\right\} \tag{12}$$

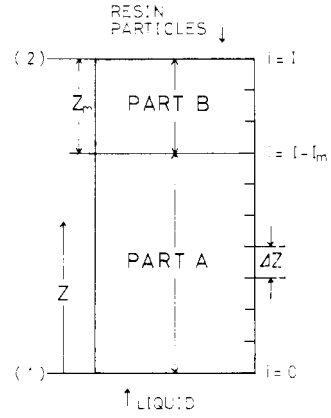

Figure 1. Diagram of ion exchange column

The conditions for $y_{i,j+1}$ given by Equation 10 to be positive and not greater than unity will be found by combining Equation 10 with Equation 8 as follows:

$$y_{i,j+1} = F_3 x_{i,j} + \left(y_{i,j} - \frac{F_3 y_{i,j}}{K(1 - y_{i,j}) + y_{i,j}} \right) \tag{13}$$

The conditions for $0 \leqq y_{i,j+1} \leqq 1$, the ranges of F_3 which will give the nonnegative value of the second term of the right side of Equation 13 and will also keep the possible maximum value of the right side of Equation 13 below unity, are as follows:

$$\left.\begin{aligned} F_3 &\leqq \frac{1}{K} \quad \text{for} \quad K > 1 \\ F_3 &\leqq 1 \quad \text{for} \quad K = 1 \\ F_3 &\leqq K \quad \text{for} \quad K < 1 \end{aligned}\right\} \tag{14}$$

In the semicontinuous countercurrent operation of the ion exchange moving bed used for this investigation, the resin bed moves downward after each period of liquid flow. Equations 3 through 5 are applied only to the liquid flow period, the time of which is designated by τ_F. Let $x_{i,1}$ represent the value of x at height $i \cdot \Delta Z$ measured from end 1 in Figure 1 at the end of the liquid flow period, and let $x_{i,2}$ represent that just after the movement of the resin bed. In other words, $x_{i,2}$ is the initial condition of x for the next liquid flow period. Assume that the column is divided into I parts along the axis, each of which is ΔZ in height, and that the resin bed moves Z_m every period. Z_m is equal to $I_m \Delta Z$, as shown in Figure 1. Then $x_{i,2}$ will be given as follows:

$$\left.\begin{aligned} x_{i,2} &= x_{i+Im,1} : i = 0 \sim I - I_m - 1 \\ x_{I-Im,2} &= \frac{\alpha x_f + \beta x_{I,1}}{\alpha + \beta} : \alpha, \beta \geqq 0 \\ x_{i,2} &= x_f : i = I - I_m + 1 \sim I \end{aligned}\right\} \tag{15}$$

where x_f is the concentration of interstitial liquid in the fresh resin particles which occupy part B in Figure 1. By selecting values of α and β, we can give any value of x between x_f and x_I, to the interface between the fresh resin particles and those remaining. The initial conditions of x_s and y for the next liquid flow period can be obtained by replacing x in Equation 15 by x_s and y, respectively.

To find the best values of α and β in Equation 15, the outlet liquid concentration, x_2, at steady state given by the numerical calculations was examined to see if it satisfies the over-all

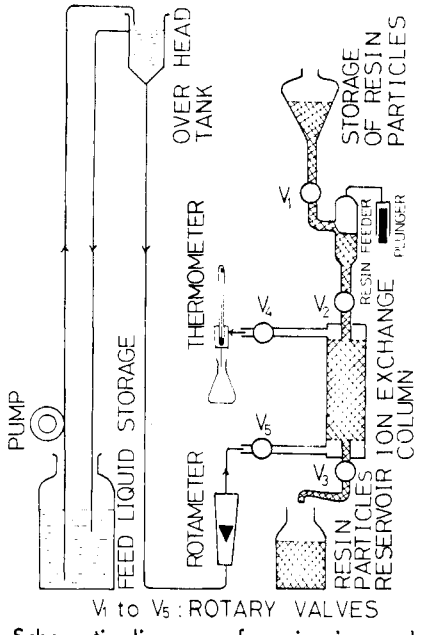

Figure 2. Schematic diagram of moving ion exchange bed

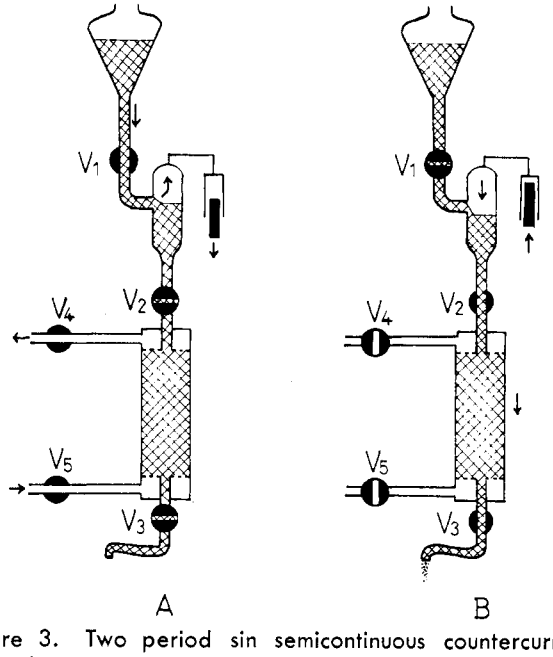

Figure 3. Two period sin semicontinuous countercurrent operation

A. Period of liquid flow
B. Period of bed movement

material balance of the column for the three cases of α and β shown below.

Case 1. $\alpha = 0$

Case 2. $\beta = 0$

Case 3. $\alpha = \beta$

The results are as follows: Case 1 is the worst of all. x_2 at the steady state differs by 20% from that given by the material balance. Case 2 is the best of all and the difference of x_2 at the steady state is less than 1%. Case 3 is between Cases 1 and 2 and the difference of x_2 at the steady state is about 10%. Case 2 was therefore adopted in this investigation.

When I_m has a small value such as 1 or 2, the numerical calculations tend to give a value of x_2 at steady state which differs by more than 1% from that expected from the material balance. The straightforward method to improve the material balance is to use a smaller ΔZ, but this increases the time of computation rapidly. By subdividing only part B in Figure 1 into a much smaller increment of Z than ΔZ, say ΔZ_m, the error in the material balance decreases, keeping the time of computation almost unchanged.

Over-all Material Balance of Column. Let subscripts 1 and 2 designate the bottom and top ends of the column, respectively, as shown in Figure 1. The over-all material balance equations are given as follows for $q_2 = 0$:

$$V_F C_1 = V_F C_2 + V_p q_1 + V_f C_1 \tag{16}$$

$$V_F C_{\Sigma 1} = V_F C_{\Sigma 2} + V_f C_{\Sigma 1} \tag{17}$$

In each period of liquid flow, the outlet liquid concentration changes with time, because the bed is essentially fixed during this period. Here the term steady state means the repetition of the same transient phenomena during each period of liquid flow. Thus, C_2, $C_{\Sigma 2}$, and q_1 are the values at the steady state averaged over the period of liquid flow.

Substituting $C_1 = C_{\Sigma 1}$, we obtain the following equations from Equations 16 and 17.

$$q_1 = R_V(C_{\Sigma 2} - C_2) \tag{18}$$

or

$$y_1 = R_V \frac{C_{\Sigma 2}}{Q}(1 - x_2) \tag{19}$$

where

$$x_2 = \frac{C_2}{C_{\Sigma 2}} \tag{20}$$

and

$$R_V = \frac{V_F}{V_p} \tag{21}$$

V_p and V_f, which appear in Equations 16 through 21, are the apparent flow rates of the resin particles and of the liquid accompanying them, respectively. They are obtained by dividing by τ_F the volumes of the resin particles and of the accompanying liquid fed after every liquid flow period.

Experimental Equipment and Method

In designing moving bed ion exchange columns, two directions of the movement for the packed resin particles may be considered. One is against gravity and the other is with it. The equipment used in this investigation was of the second type, where the flow system of particles is relatively simple. A schematic diagram is shown in Figure 2. The process of the countercurrent contact is divided into two periods as follows.

Period of Liquid Flow (Figure 3,*A*). V_2 and V_5 are opened and the fluid flows through the column. During the flow of liquid, V_1 is opened and the fresh resin particles come from the resin storage into the resin feeder as the plunger goes down. Meanwhile, V_4 and V_5 are closed. V_1 is also closed after the plunger has reached its lower dead point.

Period of Movement of Resin Particles (Figure 3,*B*). In this period, V_2 and V_3 are opened while V_1, V_4, and V_5 are closed. The resin particles bed is forced to move downward by the pushing stroke of the plunger. The fresh resin particles are fed to the top of the column as much as corresponds to the volume change of the plunger between its upper and lower dead point. The exhausted particles leave from the bottom of the column. The five valves, V_1 to V_5, are driven by the reversible electric motors whose directions

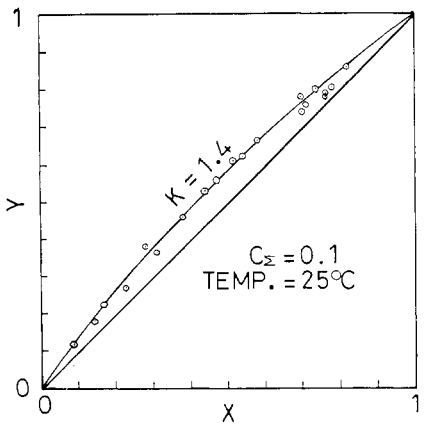

Figure 4. Equilibrium selectivity data
Amberlite IR-120 (H^+) + 0.1N NaCl

of rotation are controlled by an electric timer. The column is made of glass, the inner diameter of which is 32 mm. It has a filter at the top and the bottom where the resin particles are separated from the liquid. The resin particles are charged into or discharged from the column through the pipe attached to the top or the bottom of the column.

The cation exchange resin, Amberlite IR-120, was put into the hydrogen form, using 1 to 3N hydrochloric acid. After washing, the resin was charged to the resin storage tank with pure water. The resin slurry was transferred by pulling a vacuum on the vessel where the slurry was to be charged.

NaCl aqueous solution (0.1N) was charged to the column and the outlet liquid was analyzed for the hydrogen ion released from the ion exchange resin and for chloride ion. The sodium ion concentration was equated to the difference between the concentration of the hydrogen ion and that of the chloride ion. The amount of the sodium ion adsorbed on the ion exchange resin was estimated by a material balance equation.

Experimental Results

The experiments on the moving bed units were carried out using the ion exchange system of 0.1N NaCl aqueous solution and the hydrogen form of Amberlite IR-120, using the semicontinuous countercurrent contactor described above. The equilibrium relations of the ion exchange reaction represented by Equation 1 were measured at 25° C and the results are shown in Figure 4. From these measurements, the selectivity coefficient defined by Equation 2 was given as 1.4. The ion exchange capacity, Q, was measured as 2.95 meq per ml of swelled resin particles.

The moving bed runs were performed at room temperature ranging from 16° to 27°C. The time of the period of liquid flow, τ_F, tested in this investigation was 41, 101, 221, and 378 seconds and the time for each movement of the resin bed, τ_P, was 19 seconds for τ_F of 41 to 221 seconds or 42 seconds for τ_F of 378 seconds. The column height, Z, was 5, 10, and 20 cm. V_p was 0.0125, 0.0250, and 0.050 cm³ per sec.

x_2 at the steady state is plotted against R_V in Figure 5, which shows that neither Z, V_p, nor τ_F affects x_2. Figure 5 also shows that x_2 becomes zero for R_V less than about 30. The fact that V_F/V_p is equal to Q/C_Σ means that in an $x - y$ diagram the operating line has a slope of unity. y_1 at steady state calculated from Equation 19 is also plotted in Figure 5. y_1 is unity for R_V greater than 30 and decreases linearly to zero as R_V approaches zero. These facts suggest that for R_V greater than 30 the concentration distributions within the column may exist in a relatively narrow region around the end of the liquid outlet, so that the exhausted resin particles are saturated, as Gondo (1967) discussed from the results of numerical calculations of the moving bed of equilibrium stages. The numerical calculations using Equations 8 to 10 will make this clear.

An example of the transient change of x_2 is shown in Figure 6,A and B. It was generally difficult to determine t_s distinctly from Figure 6,A, the time consumed by the liquid flow until steady state was obtained. t_s does not contain the time spent by the bed movement. To avoid this difficulty, the data were plotted in the semilog diagram as shown in Figure 6,B, and t_s was tentatively determined as the time corresponding to point S in Figure 6,B, which is easily found as the intersection of the slanting and the horizontal lines. The t_s thus determined was divided by the residence time of liquid in the column to give θ_s, the nondimensional time of the liquid flow required for the steady state. In Figure 7, θ_s's are shown plotted against R_V. Although Figure 7 does not give a good correlation of the data, it provides some information about the transient phenomena. θ_s ranges from 130 to 400 and decreases as R_V increases. Such variables as Z and V_p seem not to have clear effects on θ_s, while smaller τ_F tends to give larger θ_s values. Figures 5 and 7 show that the characteristics of the steady and the transient states are not easily correlated with the operational variables through the graphical studies of the experimental results.

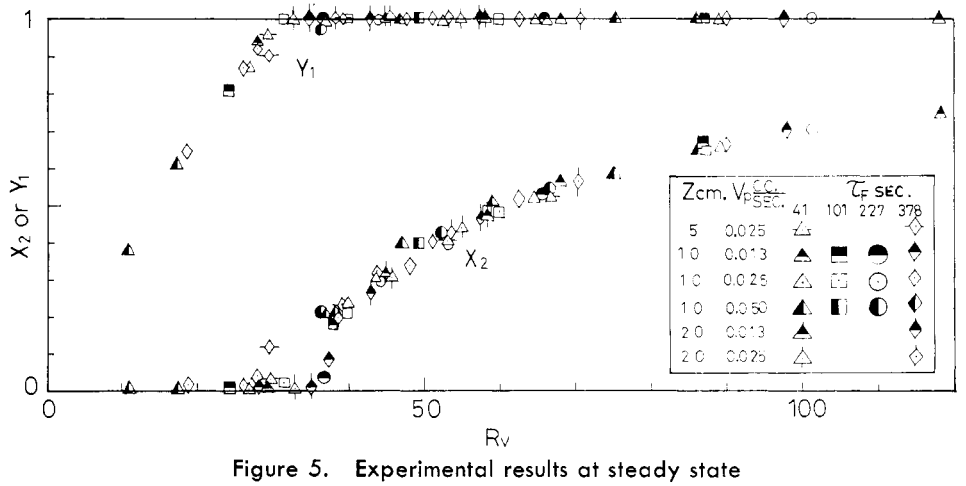

Figure 5. Experimental results at steady state
X_2. Observed
Y_1. Calculated by Equation 19

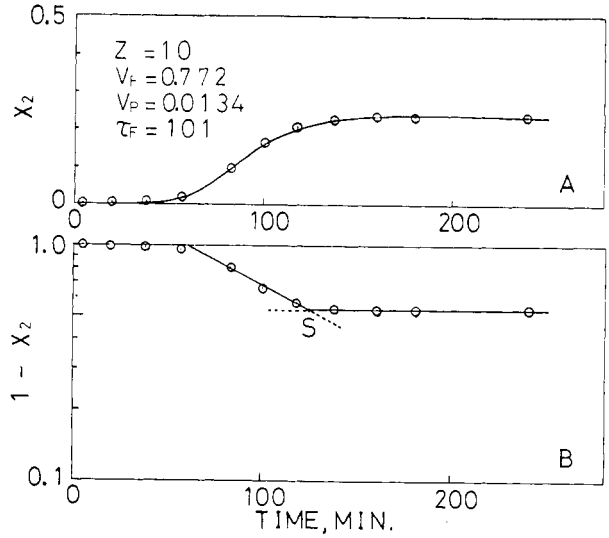

Figure 6. Example of history curve of outlet liquid concentration

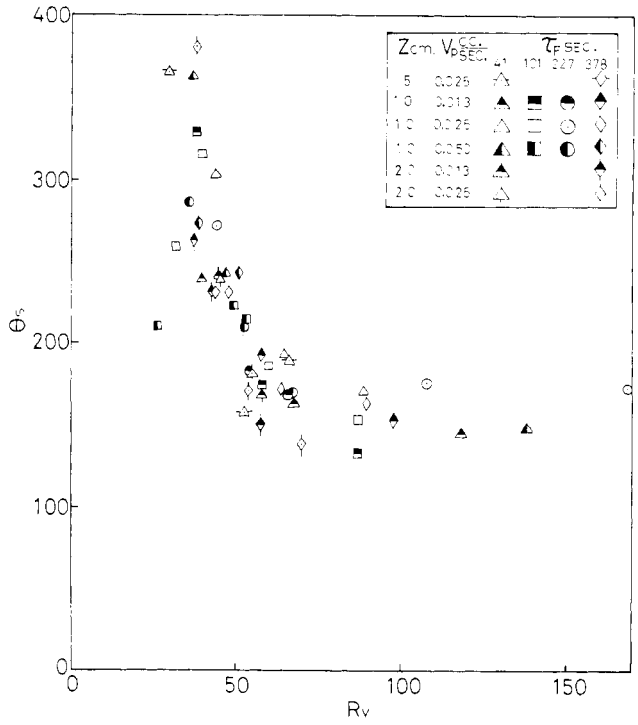

Figure 7. Variation of dimensionless time required for steady state with R_V

Numerical Calculations and Comparison of Results with Experiments

Hiester *et al.* (1956) reported that the rate-controlling step of mass transfer in ion exchange can be predicted by evaluating parameter ζ defined by Equation 22.

$$\zeta = 4.8 \frac{Q(1-\epsilon)}{C_\Sigma \epsilon} \cdot \mathrm{Pe}^{-0.5} \cdot \left(\frac{D_p}{D_F}\right) \tag{22}$$

They report that, for ζ greater than 3 the rate of mass transfer is controlled by the resistance of the liquid phase, for ζ less than 0.3 by the internal diffusion within the resin particles, and for ζ between 0.3 and 3 by both of them. In this investigation, most of the experimental conditions gave ζ greater than 3 and for the rest of them ζ was about 2. The values of the parameters used in the estimation of ζ are as follows:

C_Σ = 0.1
Q = 2.95
d_p = 0.075
ϵ = 0.34
D_F = 2.05×10^{-5} (Hiester *et al.*, 1956)
D_p/D_F = 0.19 (Hiester *et al.*, 1956)

Therefore, Equations 3 to 5 and their related difference equations can be applied to this study.

As for the estimation of k_F, the authors adopted a correlation equation proposed by Carberry (1960) not only because it had a theoretical basis but also because it is appropriate for solid-liquid mass transfer operations such as ion exchange. Carberry's correlation is given as

$$k_F = 1.15 \left(\frac{\mathrm{Re}}{\epsilon}\right)^{-1/2} \cdot \mathrm{Sc}^{-2/3} \cdot \frac{u_F}{\epsilon} \tag{23}$$

The restrictions for the range of F_1 to F_3 given by Equations 12 and 14 must be remembered in selecting the magnitude of Δt and ΔZ. ΔZ_m was taken as one fifth of ΔZ in case of I_m of 1 or 2. Figure 8 shows examples of the computational results compared with the experimental data. In Figure 8, the values of x_2 at the steady state obtained experimentally agree with the predicted values. The predictions of the data in the transient state are satisfactory for large I_m values. For relatively small I_m values, the calculation gives the time required for the steady state about 10 to 20% less than that observed. The concentration profile may be deformed at the interface of parts A and B shown in Figure 1 through the disorders of the packed resin particles caused by the flow of the charged resin particles into the top of the column. This deformation of the concentration profile might result in larger t_s than that expected theoretically. For large I_m, such an effect caused by the mixing of the resin particles may not be so severe as for small I_m and may result in better agreement of the computational predictions with the experimental data. The other reason for the disagreement in case of small I_m could be the contribution of mass transfer during the resin movement. This was neglected in the calculations. This contribution must be relatively small for large τ_F, but may be large for small τ_F—that is, for small I_m.

However, the method of numerical calculations derived here can predict fairly well the phenomena of the moving bed from a practical point of view, especially when I_m is large enough.

The concentration profiles at steady state generally take the form shown in Figure 9, where the concentration changes from its inlet value to its outlet one within relatively short height compared to the height of the column. This may be why the column height had no effect on experimental values of x_2, as shown in Figure 5.

As for the effect of τ_F on the phenomena, numerical calculation gives clear differences of the concentration profiles between τ_F = 41 and 378 seconds, as shown in Figure 9, and comparison of Figure 8,*C*, with Figure 8,*D*, shows that smaller τ_F values give larger θ_s values, as observed in the experiments.

As R_V approaches 30, the concentration profiles tend to spread all over the column. An example is shown in Figure 10.

Conclusions

Experiments and computational studies were performed for the moving ion exchange bed using the ion exchange sys-

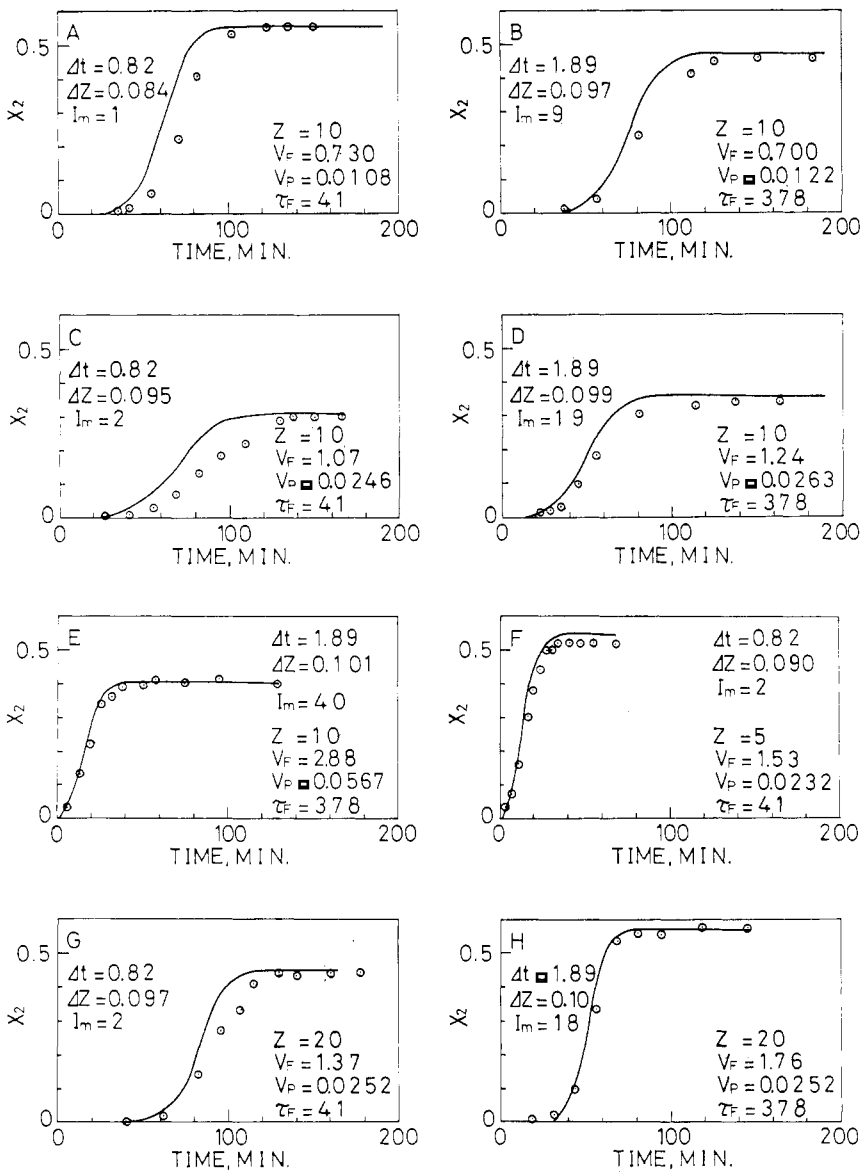

Figure 8. Comparisons of numerical calculations and experiments

$C_\Sigma = 0.1, X_1 = 1, X_f = 0, Y_2 = 0$

— Calculations by digital computer

○ Experimental data

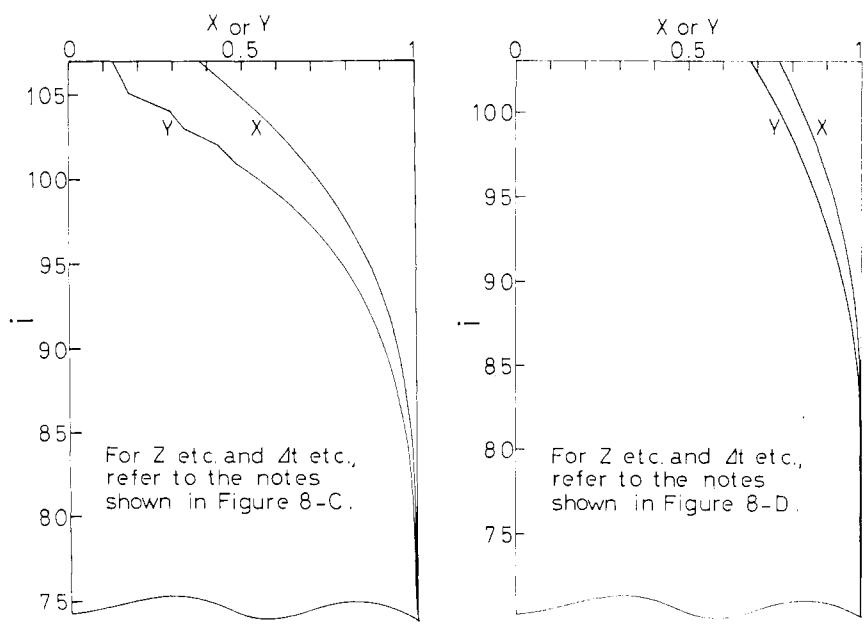

Figure 9. Concentration distribution curves at steady state

Patterns just before bed starts moving downward

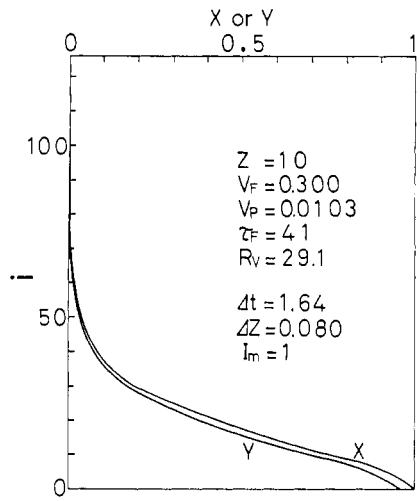

Figure 10. Spreading of concentration distribution curves at R_V close to Q/C_Σ

Patterns just before bed starts moving downward

tem of the sodium ion, the hydrogen ion, and the strong cation exchange resin, Amberlite IR-120.

The results show that the outlet liquid concentration depends on R_V but not on Z, τ_F, and the absolute value of V_F or V_p. They also show that θ_s, the nondimensional time required for the steady state, ranges from 130 to 400, decreasing with an increase of R_V, and that smaller τ_F tends to give larger θ_s.

To simulate the phenomena observed in the experiments, numerical calculations of the material balance equations were derived and carried out with k_F given by Carberry's correlation, assuming that the resistance of liquid phase is rate-controlling.

The results of simulation were satisfactory for large I_m values, but for small I_m values there were considerable differences between theory and experiments. However, the method of simulation derived here might be useful for appropriate predictions of the phenomena.

Nomenclature

a = surface of particles per unit volume of packed bed, equal to $6(1 - \epsilon)/d_p$ for spheres d_p in diameter, cm²/cc
C = liquid concentration of Na^+, meq/cc
C_Σ = total cation concentration of liquid phase, meq/cc
d_p = average diameter of resin particles, cm
D_F = ionic diffusivity in liquid phase, cm²/sec
D_p = ionic diffusivity in resin particles, cm²/sec
F_1, F_2, F_3 = constants defined by Equation 11, dimensionless
i = number of ΔZ, dimensionless
I = $Z/\Delta Z$
I_m = $Z_m/\Delta Z$
j = number of Δt, dimensionless
k_F = mass transfer coefficient of liquid phase, cm/sec
K = selectivity coefficient, dimensionless
Pe = Peclet number, $d_p u_F/6(1 - \epsilon)D_F$, dimensionless
q = concentration of Na^+ in resin particle, meq/cc
Q = ion exchange capacity, meq/cc, of swelled resin particles
Re = Reynolds number, $d_p u_F \rho/\mu$, dimensionless
R_v = V_F/V_p
Sc = Schmidt number, $\mu/\rho D_F$, dimensionless
t = time, sec
t_s = time required for steady state, sec
Δt = time increment, sec
u_F = superficial velocity of liquid, cm/sec
V = volumetric flow rate, cc/sec
x = equivalent fraction of Na^+ in liquid phase, dimensionless
y = equivalent fraction of Na^+ in resin phase, dimensionless
Z = column height or coordinate along axis of column, cm.
ΔZ = increment of column height, cm
α, β = factors in Equation 15, dimensionless
ϵ = void fraction of packed bed, dimensionless
ζ = parameter defined by Equation 22
θ_s = dimensionless time required for steady state, dimensionless
τ_F = time of liquid flow period, sec
τ_p = time of bed movement period, sec
μ = viscosity of liquid, g/cm/sec
ρ = density of liquid, g/cc

Subscripts

F = liquid
f = liquid accompanying resin particles
p = resin particles
s = interface between liquid and resin particles
1 = bottom end of column
2 = top end of column

Literature Cited

Carberry, J. J., *A.I.Ch.E. J.* **6**, 460 (1960).
Drake, G. M., Jr., Peebles, F. N., U. S. Atomic Energy Commission, **AECU-3463** (1957).
Gondo, S., *Mem. Fac. Eng., Kyushu Univ.* **26**, 103 (1967).
Hancher, W. C., Jury, S. H., *Chem. Eng. Progr. Symp. Ser.* **55**, No. 24, 87 (1959).
Hiester, N. K., Stanford Research Institute Tech. Rept. **6**, SRI Project No. CU-337 (March 30, 1951).
Hiester, N. K., Fields, E. F., Phillips, R. C., Radding, S. B., *Chem. Eng. Progr.* **50**, 139 (1954).
Hiester, N. K., Phillips, R. C., U.S. Atomic Energy Commission, AECU-2742 (1953).
Hiester, N. K., Radding, S. B., Nelson, R. L., Jr., Vermeulen, T., *A.I.Ch.E. J.* **2**, 404 (1956).
Higgins, I. R., Oak Ridge National Laboratory, **ORNL-1918** (1956).

Received for review September 19, 1969
Accepted October 20, 1970